# Novel 3D-printed microfluidic magnetic platform for rapid DNA isolation

Güneş Kibar, $^{\dagger,\P}$  Büşra Sarıarslan, $^{\S,\P}$  Serkan Doğanay, $^{\parallel}$  Gökay Yıldız, $^{\perp}$  O. Berk Usta, $^{\ddagger,\#}$  and Barbaros Çetin $^{*,\S,\P}$ 

†Dept. Materials Sci. & Eng., Adana Alparslan Türkeş Science and Technology University,

Adana 01250 Türkiye

‡Center for Engineering in Medicine and Surgery, Department of Surgery, Massachusetts General Hospital, Harvard Medical School, Boston 02114 MA, USA

¶UNAM – National Nanotechnology Research Center and Inst. Materials Sci. Nanotech.

Bilkent University, Ankara 06800 Türkiye

§Microfluidics & Lab-on-a-chip Research Group, Mech. Eng. Dept.

Bilkent University, Ankara 06800 Türkiye

 $\|\mathit{Mechatronics\ Eng.\ Dept.\dot{I}zmir\ Katip\ Celebi\ Uni.,\ \dot{I}zmir\ 35620\ T\ddot{u}rkiye}$ 

⊥TEKGEN Healthcare Services Inc., Ümraniye, İstanbul 34775 Türkiye

#Shriners Children's Hospital, Boston 02114 MA, USA

E-mail: barbaros.cetin@bilkent.edu.tr

Phone:  $+90(312)290\ 2108$ 

#### Abstract

This study presents a novel miniaturized device as a 3D-printed microfluidic magnetic platform specifically designed to manipulate magnetic microparticles in a microfluidic chip for rapid DNA isolation. The novel design enables the movement of the magnetic particles in the same or opposite directions with the flow or suspending them

in a continuous flow. A computational model was developed to assess the effectiveness of magnetic manipulation of the particles. Superparamagnetic monodisperse silica particles synthesized in-house are utilized for the isolation of fish sperm DNA and human placenta DNA. It was demonstrated that the proposed platform can perform DNA isolation within 10 minutes with an isolation efficiency of 50% at optimum operating conditions.

## Introduction

The purification or isolation of biological samples, especially deoxyribonucleic acid (DNA), which is a biological information storage molecule, is crucial and a starting point for many genetic studies, <sup>1</sup> forensic science, <sup>2</sup> and clinical diagnosis of rare diseases, <sup>3</sup> cancer <sup>4</sup> and/or virus-based sicknesses. <sup>5–7</sup> So far, many different techniques such as size exclusion chromatography (SEC), <sup>8</sup> ion-exchange chromatography (IEC), <sup>9</sup> affinity chromatography (AC), <sup>10</sup> alkaline extraction, <sup>11</sup> salting-out method, filter papers, <sup>12</sup> silica matrices (gels, resins or beads), <sup>13</sup> magnetic beads <sup>14</sup> (with commercially available forms in packed-column, gravity column, spin-column, spin-plates, and magnetic stands) have conveniently been employed to isolate DNA. DNA isolation techniques commonly rely on adsorption-desorption mechanisms via solid-phase extraction, electrostatic interactions, or sequence-specific capture. <sup>15</sup> The suitable method of choice depends on the quality and quantity of isolated DNA, required sample amount and laboratory equipment for the protocol, desired yield, time and cost constraints, as well as the necessary technical expertise.

In daily practice, extraction methods have already been developed into commercial kits for laboratories. <sup>16</sup> Commercial DNA extraction kits have shown successful results with satisfactory yield; <sup>17</sup> however, reducing the analysis time for every extraction is still desirable. For example, even though the centrifugation process takes about a minute for adsorption (binding of DNA), wash, and desorption (eluting DNA) steps in the protocol of spin-column-based DNA purification (e.g., Qiagen-QIAamp<sup>®</sup>, NucleoSpin Tissue Kit, Puregene DNA

Purification System, UltraClean<sup>TM</sup>, BloodSpin<sup>TM</sup> Kit, GFX<sup>TM</sup> Genomic Blood DNA Purification Kit), the overall isolation process resulted in approximately 30 minutes to one hour for each sample considering sample loading/incubating, adding/removing regent between centrifugation steps. <sup>18–20</sup> Rapid molecular assays are still a bottleneck in most clinical applications where large sample sets need to be processed within a limited time, as we have recently experienced during the COVID-19 pandemic. In this regard, magnetic bead-based approaches are faster and more cost-effective for each run than spin-column-based methods. <sup>21</sup> Commercial kits typically require a sample volume of somewhere between 200 μL and couple mL to process <sup>22</sup> (especially, the minimum requirement for the sample volume may be quite challenging for specific applications such as forensic) and technical expertise to run the workflow and expensive bench-top specialized equipment, such as high-pressure pumps or high-performance liquid chromatography (HPLC) systems. <sup>23</sup> Moreover, some commercial kits may not be available in certain low-resource settings and countries. <sup>24</sup> These drawbacks of conventional methods push clinical and research laboratories to address these shortcomings, ensure continuous development, and find alternative solutions with emerging technologies.

Alternative to conventional methods, microfluidic systems offer miniaturization of labscale applications that allow operating at a few µL or even nL and achieving better accuracy, reduced analysis time as well as higher reliability of the entire isolation process with
minimizing the risk of cross-contamination. <sup>25,26</sup> The ability to precise control of fluid at the
micro-scale has opened up numerous possibilities for replacing batch-top equipment with continuous flow processes and various functional components such as channels, valves, pumps,
mixers, and sensors in the microfluidic systems. <sup>27–30</sup> Over the recent years, microfluidic isolation of DNA evolved from micro-capillary chromatography columns <sup>31,32</sup> to microfluidic
devices and platforms in various designs such as cartridges, <sup>33,34</sup> centrifugal devices (so-called
lab-on-a-disc), <sup>35–37</sup> glass <sup>38</sup> and PDMS microchips. <sup>39–41</sup> Microfluidic platforms incorporating surface-modified magnetic beads enable the selective purification of targeted DNA from
other substances under the influence of a magnetic field created by electromagnets. <sup>42,43</sup> in-

tegrated soft magnets <sup>44,45</sup> or external permanent magnets. <sup>46</sup> Electromagnets flexibly control the magnitude and form of the magnetic field; however, the heat generation due to the coil-carrying current results in a deterioration of the stability of the magnetic field, especially when strong magnetic fields are required. <sup>47</sup> Fabricating integrated chips is more complex and expensive for trials with biological samples. Alternatively, external permanent magnets are cheap and easy to access. They are favorable to employ when a rapid spatial change is required to generate strong magnetic forces. <sup>48</sup> Moreover, they could be placed separately near the microfluidic devices, and are ideal for controlling the motion of the magnetic beads for reusability and reproducibility of each experiment. <sup>49</sup>

The manipulation of magnetic beads in microfluidic channels could be classified as (i) immobilized beads (static magnetic bead chains), (ii) temporarily immobilized beads (dynamic magnetic bead chains, magnetic beads in microwell, magnetic fluidized bed), and (iii) actively transported beads (magnetophoresis, magnetic droplet). In the first group, the beads are used as a static, stationary phase for separation in the microfluidic channel. Switching-on magnetic fields locally capture them so as not to drag away any beads during sequentially flushing with different reagents in the microchannel. 46,50 The beads are retained in the channel wall, forming a diffusion barrier.<sup>51</sup> In the second group, to overcome this drawback, the beads are locally trapped by the magnetic field and re-suspended by switching off or removing the magnetic field to efficiently wash the beads. 52-55 The movement of the magnetic beads in a microfluidic channel provides magnetic mixing and increases the effective specific surface area, but the motion of the beads is challenging to control under the on-off magnetic field and flow. In the third group, the beads are actively transported in a microfluidic channel without stopping the flow; however, the successful bead transport is highly sensitive and depends on the active control of magnetic field strength, orientation, and flow rate of the reagents. For example, bead accumulation in the microchannel could block the channel or outlet position of the beads depending on the flow during prolonged processes. 56,57

In this study, we propose a novel magnetic platform as an innovative solution for manipulating the super-paramagnetic beads for rapid DNA isolation in a spiral microfluidic device. <sup>58</sup> A computational model was developed to assess the positioning and rotation of the permanent magnets on the platform. Following the design phase, the magnetic platform was 3D printed and assembled with permanent magnets and necessary electronic components. The spiral microfluidic channels were fabricated using polydimethylsiloxane (PDMS) mold-The super-paramagnetic monodisperse silica microbeads were synthesized in-house. The magnetic platform enables the manipulation of super-paramagnetic microbeads within a spiral microchannel in the same/opposite direction of the magnetic field or microbeads to be suspended in the continuous flow. We tested our platform by performing binding, washing, and elution steps to isolate the fish sperm and human placenta DNAs in a continuous flow. The effect of flow rate and isolation parameters such as DNA concentration and pH of elution buffer were analyzed. Our platform can handle the DNA isolation within about ten minutes with a sample volume of 10 µL without any need for sophisticated hardware. In this regard, we believe that our platform would be a viable alternative to conventional techniques and have a crucial impact on future automated point-of-care testing, especially considering the rapid analysis time. The comparison of different aspects of our platform with other techniques available in the literature is given in Table 1.

### Materials and Methods

To evaluate the magnetic force generated by the permanent magnet in the microfluidic chip region, a 3D numerical model was built by COMSOL Multiphysics<sup>®</sup>. The details of the computational model and the relevant results are given in Supporting Information.

#### Particle synthesis and characterization

The superparamagnetic monodisperse silica particles were synthesized via staged-shape templated hydrolysis and condensation protocol. <sup>31,59,60</sup> The template carboxyl-carrying monodisperse polymeric particles of around 6 µm were synthesized via multi-stage polymerization and magnetized as described in the literature. <sup>61</sup> Then, the 0.4 g of magnetic polymeric template particles were dispersed in 50 mL isopropanol containing 0.25 g TBAI (tetrabutylammonium iodide, Sigma-Aldrich), 5 mL DDI water, and 0.25 mL NH<sub>4</sub>OH (ammonium hydroxide solution, Sigma-Aldrich). This medium was mechanically stirred at room temperature for one hour at 400 rpm. The silica precursor 1.25 mL TEOS (tetraethyl orthosilicate) and 3.75 mL isopropanol were mixed and gradually introduced drop by drop into the medium containing particles. The particles and silica precursor were mechanically stirred at 30°C for 24 hours. The silica-coated magnetic polymeric particles were collected by a natural magnet and washed with isopropanol and DDI water several times. The hybrid particles were dried at 80°C overnight and then calcinated up to 450°C for six hours with a heating rate of 2°C/min to remove organic parts of the particles. The synthesized particles were morphologically, chemically, and magnetically characterized. The morphology and surface chemistry of the particles were determined using a scanning electron microscope with energy-dispersive X-ray spectroscopy (SEM-EDX Quanta 450 Akishima, Tokyo, Japan). The chemical structure was evaluated by Fourier-transform infrared spectroscopy (FTIR) (Thermo Scientific NicoletTM, USA). The magnetic character of the particles was determined by a vibrating sample magnetometer (VSM-Cryogenic Limited Model: PPM system, UK).

#### Device fabrication

The constituent elements of the platform were fabricated by a 3D-printer (Creality Ender-3). The assembled structure encompasses a brushless motor that imparts rotational motion to the segment with embedded permanent magnets beneath the microfluidic chip. The brushless motor's rotation determines the magnetic field's rotation, which determines the direction of

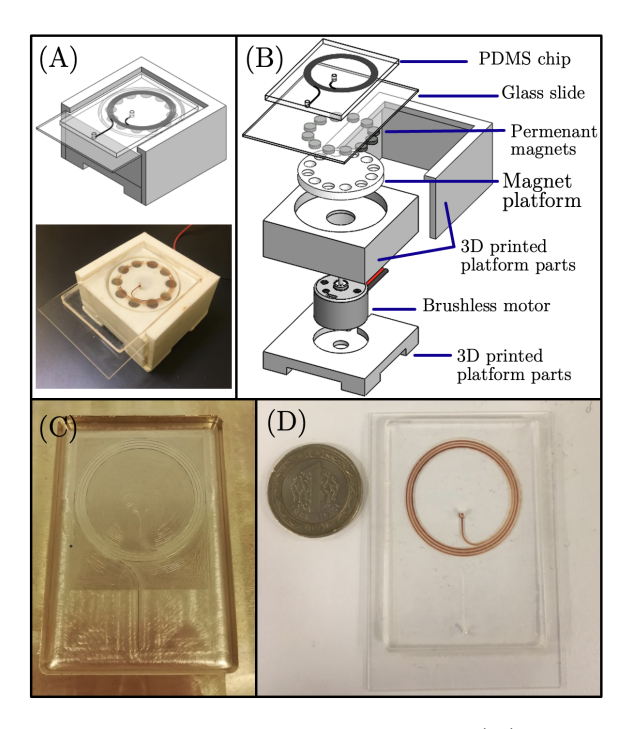


Figure 1: (A) The CAD model and 3D-printed platform, (B) exploded CAD drawing of the platform, (C) metal mold used for PDMS molding and (D) microfluidic chip (diameter of the coin is 26.15 mm)

the magnetic force on the particles. The rotational speed of the brushless motor was adjusted via the applied voltage to achieve the desired rotational speed, which led to the suspension of the particles in the microfluidic chip. These elements were then integrated into a unified structure, illustrated in Fig. 1. The fabrication of the microfluidic chip was performed by standard polydimethylsiloxane (PDMS) molding procedure,  $^{62-64}$  which was then followed by bonding to a glass slide via surface plasma treatment. The microfluidic chip has a spiral microchannel with a cross-sectional dimension of 200  $\mu$ m×400  $\mu$ m and extends to an overall length of 0.42 m. Including the inlet and the outlet sections, the microfluidic chip has a volume of about 40  $\mu$ L.

## Experimentation

The rotation of the magnetic field determines the direction of the magnetic force on the particles; therefore, the rotation direction was selected to obtain a magnetic force in the opposite direction of the drag force induced on the magnetic particles due to the flow field, which led to the suspension of the particles in the microfluidic chip. Therefore, characterization experiments were conducted to determine the required voltage for the brushless motors, hence the rotational velocity of the magnetic platform for a given volumetric flow rate inside the microfluidic chip to suspend the particles was obtained. In these experiments, the motion of the particles was inspected under the microscope (PSARON-FluidoScope, Ankara, Türkiye) to ensure the suspension of the magnetic particles at each corresponding voltage and flow rate value. For the flow rates considered in this study (5–20  $\mu$ L/min), the required voltage was determined as 1.2–2.0 V, which corresponds to a rotational speed of 1000–2000 rpm.

Two different DNA samples were used for the isolation in the microfluidic system. First, the Deoxyribonucleic acid sodium salt from salmon testes (D1626-Sigma) was employed. Different concentrations of fish sperm DNA were prepared in binding medium 1×TE (10 mM Tris, 1 mM EDTA) buffer (pH 6.0) containing 6M Guandium Hydrochloride (Gu-HCl) from 0.2 mg/mL to 40 mg/mL by dilution. Second, the Deoxyribonucleic acid from the human placenta (COT Human DNA 11581074001-Roche) was prepared in the binding medium from 6 mg/mL to 40 mg/mL by dilution. The preparation and dilution were checked using Nanodrop<sup>TM</sup> 2000/2000c (Thermo Fisher Scientific, USA. Lower detection limit: 2 ng/μL<sup>65</sup>) three times for each reading.

Superparamagnetic silica microparticles (1 mg) were loaded into the PDMS-based microfluidic chip (Fig. 1D). The particle-loaded microfluidic chip was placed over the magnetic platform (Fig. 1A). The magnetic field was generated by rotating the magnets under the microfluidic chip. A syringe pump (New Era type 1002X, Farmingdale, NY, USA) delivered the buffer solutions into the microfluidic device with the desired flow rate (5–20 μL/min). At the beginning of each experiment, the particles were washed with binding medium 1×TE (10 mM Tris, 1 mM EDTA) buffer (pH 6.0) containing 6M Gu-HCl at 20 μL/min for 2 min to prepare the system for isolation. The DNA isolation was performed in three main steps: (i) adsorption, (ii) washing, and (iii) elution. During adsorption, a 10 μL DNA sample with

known-concentration in binding buffer was transferred into a 1.0 mL insulin syringe containing binding buffer by withdrawing. Then, the sample was fed to the microfluidic system for a certain time duration (5–20 minutes) depending on the sample flow rate, during which the DNA sample was absorbed by magnetic silica particles within the microfluidic system. The adsorption medium passed through the microfluidic system and was collected as 100  $\mu$ L into the Eppendorf tube at the system outlet. Next, the washing step was applied using a washing buffer 4:1 (v/v) isopropanol/water mixture. The washing buffer was fed to the system for a certain time duration (4–16 minutes) depending on the flow rate, and the processed sample was collected as 80  $\mu$ L into the Eppendorf tube. At the last step, the elution of adsorbed DNA was accomplished by feeding the 1×TE (10 mM Tris, 1 mM EDTA) buffer (pH 8.0). The 100  $\mu$ L desorbed DNA was collected into the Eppendorf tube at the system outlet. The same protocol was followed and repeated three times for each concentration of different DNA samples.

The samples were analyzed using Nanodrop<sup>TM</sup> 2000-3300 Fluorospectrometer (Thermo Fisher Scientific, USA), and the adsorption capacity was determined as follows:

DNA adsorbed = 
$$\frac{c(\text{DNA})_{\text{initial}} - c(\text{DNA})_{\text{residual}}}{m(\text{MNs})} \times \text{Vol}$$
(1)

where  $c(\text{DNA})_{\text{initial}}$  and  $c(\text{DNA})_{\text{residual}}$  represents the DNA concentrations [mg/mL] initially loaded into the system and collected at the adsorption step, respectively. m(MNS) indicates the mass [mg] of the magnetic silica particles, and Vol denotes the volume [ml] of the sample. Sips model, which is a hybrid, three-parameter isotherm model combining the Langmuir and Freundlich models and can describe both homogeneous and heterogeneous systems, is implemented as:  $^{66}$ 

$$q_e = \frac{q_m K_S C_e^{n_S}}{1 + K_S C_e^{n_S}} \tag{2}$$

where  $C_e$  [mg/mL] is the equilibrium concentration of adsorbed DNA.  $q_e$  [mg/mg] is the amount of the DNA adsorbed per unit weight of magnetic silica particles,  $q_m$  [mg/mg] is the

maximum adsorbed DNA amount per unit weight of the adsorbent, and  $K_S$  [mL<sup>n<sub>S</sub></sup>/mg<sup>n<sub>S</sub></sup>] and  $n_S$  are the Sips constants. Nonlinear curve fitting is performed by the built-in function lsqcurvefit, which utilizes a trust-region-reflective algorithm available in MATLAB<sup>®</sup>. The regression coefficient is defined as:

$$R^{2} = 1 - \frac{\sum_{j} (q_{e,j} - q_{e_{\text{predicted}}})^{2}}{\sum_{j} (q_{e,j} - \bar{q}_{e})^{2}}$$
(3)

where  $\bar{q}_e$  is the mean of the  $q_{e,j}$  data. The adsorption efficiency was defined as follows:

Adsorption eff. = 
$$\frac{m(DNA)_{adsorbed}}{m(DNA)_{initial}}$$
 (4)

where

$$m(DNA)_{adsorbed} = m(DNA)_{initial} - m(DNA)_{residual}$$
 (5)

where  $m(DNA)_{initial}$  and  $m(DNA)_{residual}$  are the mass of initial and residual DNA.

Systematic experiments were conducted to assess the effect of pH on desorption efficiency. Elution buffer  $1\times TE$  (10 mM Tris, 1 mM EDTA) with different pH values (7.0, 8.0 and 9.0) was prepared. The isolation protocol ran with fish sperm DNA at 10  $\mu$ L/min, and each test at every pH value was repeated three times. The samples were collected as described in the protocol and analyzed using Nanodrop<sup>TM</sup> 2000-3300 Fluorospectrometer to calculate the desorption efficiency as:

Desorption eff. = 
$$\frac{m(\text{DNA})_{\text{desorbed}}}{m(\text{DNA})_{\text{adsorbed}}}$$
 (6)

where  $m(DNA)_{desorbed}$  represents the amount of DNA (ng) obtained at the elution step as collected DNA amount in the system. The isolation efficiency of the system was defined as:

Isolation eff. = Adsorption eff. 
$$\times$$
 Desorption eff. (7)

To assess the isolation efficiency of the platform, the experiments were conducted at three different flow rates and repeated three times at each flow rate.

### Results and Discussion

The magnetic silica particles were obtained morphologically spherical and monodisperse around 6 μm in SEM images at 15000×, 30000×, and 80000× magnification 5 μm, 2 μm, and 1 μm bars respectively (Fig. 2B). The surface chemistry contains O, Si, and Fe atoms with 51.03%, 33.02%, and 15.95% in weight, respectively (Fig. 2B). The FTIR spectrum showed the chemical structure of the magnetic silica beads in Fig. 2C. The peak at 1060 cm<sup>-1</sup> represents the Si–O–Si bond in the structure. <sup>64,67</sup> The absorption bands at 630 cm<sup>-1</sup>, 570 cm<sup>-1</sup>, and 440 cm<sup>-1</sup> belong to iron nanoparticles (Fe–O stretching). <sup>64,67</sup> The magnetic character of the particles was evaluated by the hysteresis curve obtained via VSM analysis (Fig. 2D). The hysteresis curve exhibited the superparamagnetic character with approximately 10 emu/g magnetic saturation. In addition, iron oxide nanoparticles (SPION) coated silica microparticles showed no permanent magnetization on coercivity.

Microfluidic DNA isolation was performed with two different DNA types as model DNA: fish sperm DNA and human Placenta DNA at different concentrations. The isolation protocol was first conducted with Fish sperm DNA at a flow rate of 10  $\mu$ L/min for each step. The isolation finished within 30 min (10 min adsorption, 8 min wash, 10 min elution, and approximately 1 min syringe change). Fish sperm DNA adsorped onto the particles during the flow using the binding buffer at pH 6.0. As seen in Fig. 3A, the amount of fish sperm DNA adsorption increases with increasing the amount of loaded DNA. After a certain amount of DNA, the adsorbent (magnetic silica particles) reaches the saturation point and exhibits no further adsorption of adsorbate molecules (DNA), which leads to the maximum adsorption capacity ( $q_m$ ). The adsorption efficiency curve showed the experimental  $q_m$  of around 100  $\mu$ g/mg particle (Fig. 3A). The Sips adsorption model was also applied to understand the

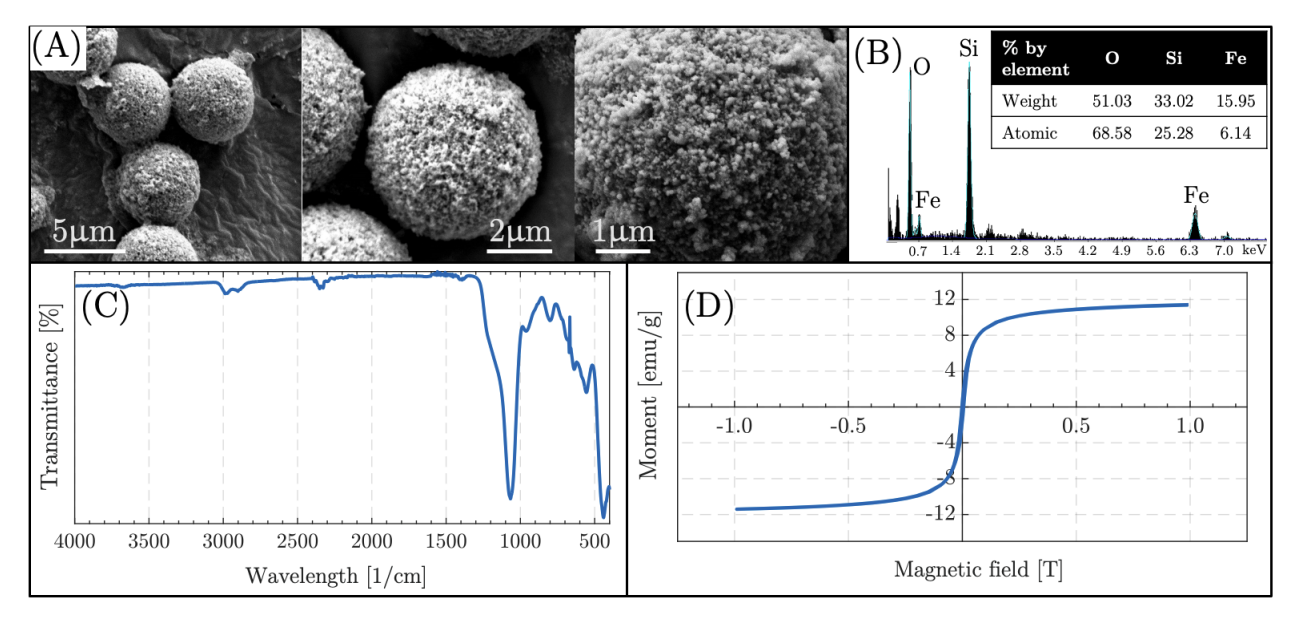


Figure 2: (A) Morphological structure (SEM images), (B) surface chemistry (EDX results), (C) chemical structure (FTIR spectrum), and (D) magnetic properties (VSM results) of synthesized magnetic particles

behavior of the adsorption process. The Sips model fits the data with a regression coefficient  $(R^2)$  of 0.990 for fish sperm DNA adsorption. The  $q_m$  of the model was 121 µg/mg. The adsorption isotherm model reveals that the system may be dominated by chemical adsorption which can be considered as a monolayer adsorption process. <sup>66</sup>

Human placenta DNA was also used to understand the adsorption behavior of the system under the same conditions (at a flow rate of 10  $\mu$ L/min for each step and binding buffer at pH 6.0). The higher concentrations were chosen to determine the maximum adsorption capacity not to consume the DNA sample (Fig. 3B). The  $q_m$  was found experimentally around 110  $\mu$ g/mg which is comparable with the magnetic nanoparticles employed in several batch systems available in the literature (16–121  $\mu$ g/mg).<sup>59,68–71</sup> The Sips model fits the experimental data points with a regression coefficient of 0.998 and  $q_m$  of 109  $\mu$ g/mg, which matches the experimental data. The desorption efficiency was determined using 1×TE buffer with different pH values. The experiments were repeated three times with fish sperm DNA at 10  $\mu$ L/min and 100  $\mu$ L elution volume at room temperature (Fig. 3C). The results showed that chemical interactions also dominated the desorption step. As the elution buffer pH value

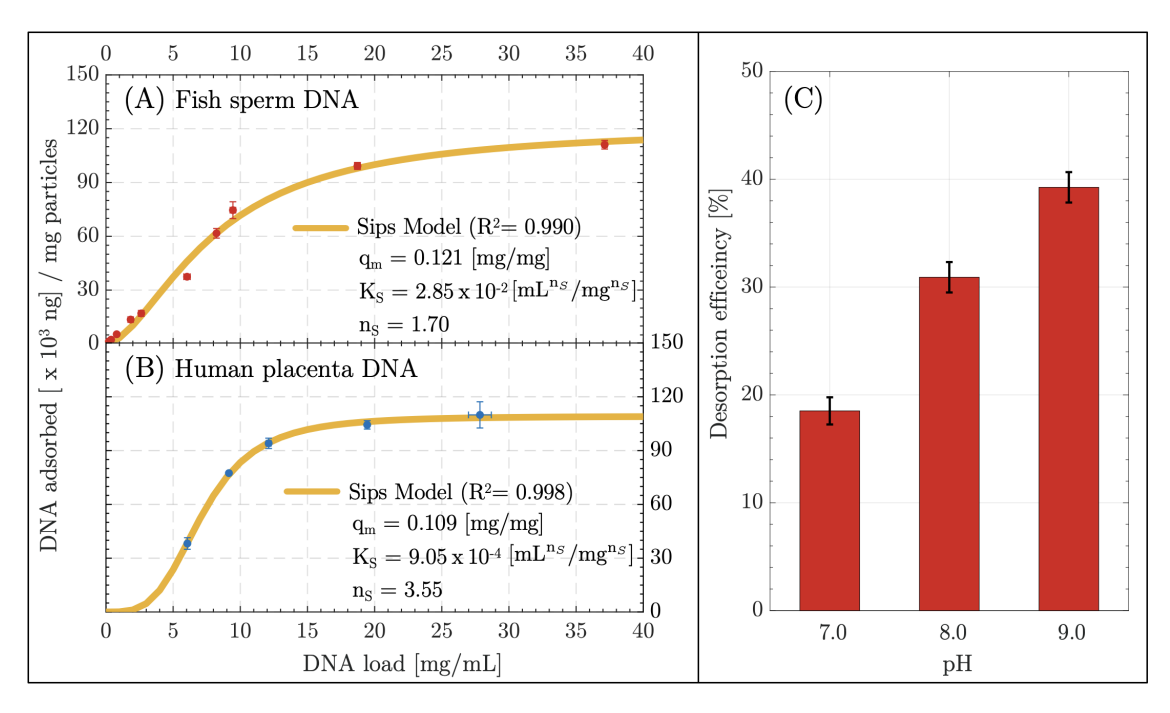


Figure 3: Adsorption capacity for (A) fish sperm DNA and (B) human placenta DNA. The values are the mean values with  $\pm$  standard error from three independent repeated experiments at each flow rate (Sample flow rate: 10  $\mu$ L/min). (C) Desorption efficiency of fish sperm DNA for different pH. Three repeated experiments at each pH value (Sample flow rate: 10  $\mu$ L/min).

increased from 7.0 to 9.0, desorption efficiency also increased from 18% to 38%.

The effect of flow rate on isolation steps was investigated using fish sperm DNA as model DNA with a binding buffer of pH 6.0 and an elution buffer of pH 8.0 to compare similar materials and methods utilized for DNA isolation. For this reason, three repeated experiments were performed at a flow rate of 5  $\mu$ L/min, 10  $\mu$ L/min, and 20  $\mu$ L/min. As seen in Fig. 4, the adsorption efficiency is inversely proportional to the flow rate, and the adsorption performance reaches saturation at the flow rate of 10  $\mu$ L/min at about 70%. Upon reaching saturation, the magnetic particles no longer have the capacity to bind additional DNA which leads to a plateau in adsorption efficiency. As the flow rate reduces, the residence time of the DNA buffer inside the microchannel that affects the contact time between the particles' surfaces and DNA molecules increases which may influence the adsorption kinetics and the electrostatic interactions, and hence improves DNA adsorption. <sup>72,73</sup> Moreover, the drag force on the particles also decreases which eases the attachment of the DNA molecules

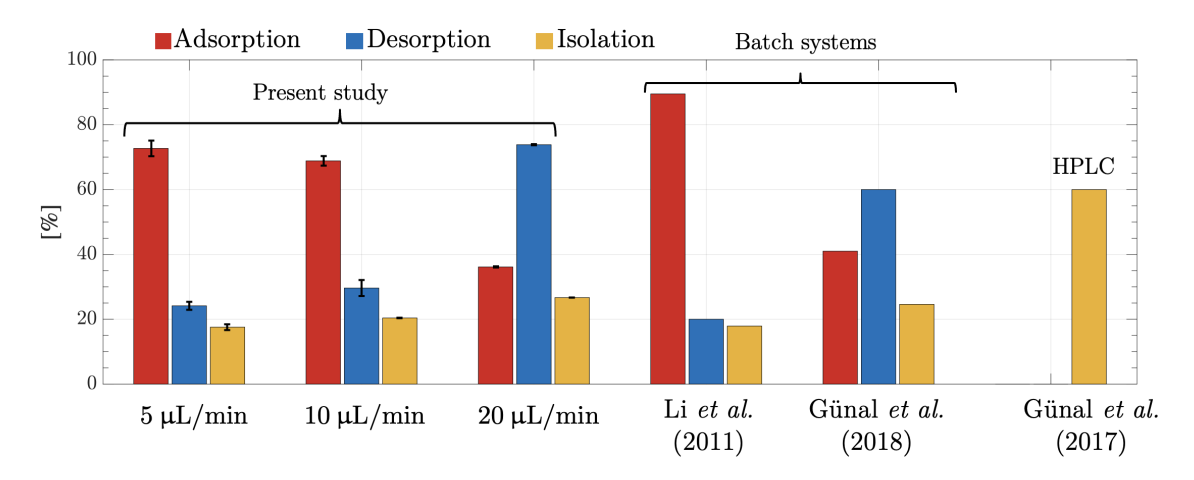


Figure 4: Adsortion, desorption and isolation efficiencies of the platform for fish sperm DNA at different flow rates. The values are the mean values with  $\pm$  standard error from three independent repeated experiments at each flow rate. Results of other studies available in the literature  $^{31,59,68}$  is also given for comparison.

onto the particles. When the desorption performance is assessed, it can be clearly seen that desorption efficiency increases with increased flow rate which reaches about 75% at the flow rate of 20  $\mu$ L/min. This can be attributed to the enhancement of the drag force acting on the DNA molecules which facilitates the detachment from the particles' surfaces. For rapid DNA isolation, the overall operation time needs to be kept at a minimum. The system achieved the best adsorption efficiency at 5  $\mu$ L/min, and the best desorption efficiency at 20  $\mu$ L/min. However, the adsorption efficiency for 10  $\mu$ L/min is also close to that of 5  $\mu$ L/min. In light of these findings, at optimum operating conditions to ensure shorter process time, the adsorption step can be run at 10  $\mu$ L/min, and the wash and desorption steps can be run at 20  $\mu$ L/min, which would lead to an operation time of 10 minutes (5 min adsorption, 2 min wash, 3 min elution) with an expected isolation efficiency above 50%.

The comparison of different aspects of our platform with other techniques available in the literature is given in Table 1. Although there are methods with superior isolation efficiency than that of our platform, considering the amount of sample, loaded sample and process time, our platform has superior performance. However, there is still room for improvement, especially in the desorption process. In the literature, there are studies in which the desorption efficiency has been improved by increasing the salt amount to 1 M in elution buffer <sup>74</sup> and using phosphate buffer at elevated temperature. <sup>69</sup> Therefore, the desorption performance of our platform can further be improved which would increase the isolation efficiency. In addition, we have a 40 µL volume within our spiral microchannel, which affects process time. The volume of the microchannel, channel dimensions and flow rate may be optimized to further reduce the process time, which would ensure rapid isolation. The design of our platform is quite flexible, and actually the geometry of the microchannel can be optimized depending on the intended amount of sample to be processed.

# Concluding Remarks

In this study, a novel miniaturized device as a 3D-printed microfluidic magnetic platform is presented for rapid DNA isolation. The novel design enables the movement of the magnetic particles in a continuous flow confined by a spiral microchannel. A computational model was developed to assess the effectiveness of magnetic manipulation of the particles. Superparamagnetic monodisperse silica particles synthesized in-house are utilized for the isolation of fish sperm and human placenta DNAs. The adsorption, desorption and isolation efficiency of the platform is assessed through thorough experiments. Our experiments showed that DNA isolation can be performed within 10 minutes on our platform.

Recently, our group developed flexible hydraulic reservor (FHR)<sup>28,29</sup> for zero dead-volume sample loading into microfluidic chips. A new version of FHR with integrated valve is under development. With the implementation of the newer version of the FHR, there will be no need for syringe change during the operation, which will eventually make the entire process fully-automated. Additionally, our platform has a flexible design in such a way that the volume of the FHR, and microchannel, can be modified for a specific application. Therefore, considering the excellent features such as flexible design for the amount of samples, rapid analysis, reliance on relatively less sophisticated equipment, low-cost fabrication, and most importantly, having the potential to be portable for point-of-care testing, our platform is a

viable option for low-cost, rapid DNA isolation. Further developments on the improvement of the isolation efficiency and the application of our platform for isolation of different biological materials such as bacteria, viruses, exosomes, etc. will be some of our future research directions.

# **Supporting Information**

Details of the computational model and simulation results.

# Acknowledgement

This study is financially supported by the Turkish Scientific and Technological Research Council under Grant No. TEYDEB-1170524. We also acknowledge the Turkish Fulbright Commission for a Fulbright Postdoctoral Scholarship and the Scientific and Technological Research Council of Türkiye (TÜBİTAK-2219 Award#1059B191801017) for Dr. Güneş Kibar.

Table 1: Comparison of different DNA isolation methods available in the literature

Method	Adsorbent	Adsorbate	$egin{aligned} \mathbf{Loaded} \\ \mathbf{Sample} \end{aligned}$	Isolation Eff.	$\begin{array}{c} \textbf{Isolated} \\ \textbf{DNA} \end{array}$	$\begin{array}{c} \textbf{Desorption} \\ \textbf{Volume} \end{array}$	Process time
Microfluidics <sup>31</sup> (Silica capillary)	Silica/polymeric beads	hgDNA from whole blood	120 μL Max. 12 μg (DNA)	20 – 50%	$\sim 2500 \text{ ng}$	150 μL (30 min)	$\sim$ 130 min
Microfluidics <sup>53</sup> (Glass channel)	Magnetic silica beads	Purified hgDNA and blood	$\begin{array}{c} 4~\mu L \\ 20~\mathrm{ng}~(\mathrm{DNA}) \end{array}$	20 – 70%	0.1 – 6.0  ng	$\begin{array}{c} 220~\mu\text{L} \\ (220~\text{min}) \end{array}$	18–36 min
Microfluidics <sup>42</sup> (PDMS channel)	Silica beads	HindIII-digested $\lambda$ -phage DNA	$\begin{array}{c} 20~\mu L \\ 20~\mathrm{ng}~(\mathrm{DNA}) \end{array}$	50.2%	$\sim 10 \text{ ng}$	3–6 μL (5–10 min)	15–20 min
Batch <sup>59</sup> (Eppendorf)	Silica/polymeric beads	${ m hgDNA}$	$\begin{array}{c} 1~\mathrm{mL} \\ 400~\mu\mathrm{g}~(\mathrm{DNA}) \end{array}$	25%	$\sim 100 \ \mu g/mg$ beads	$1~\mathrm{mL}$	~3 h
Qiagen spin <sup>75</sup> column (Eppendorf)	Silica medium	Plasma, serum tissue, bodily fluid	Min. 200 $\mu$ L 50 $\mu$ g (DNA)	80–100%*	$\begin{array}{c} {\rm Max.} \\ {\rm 20~\mu g/mg} \end{array}$	$50$ – $200~\mu L$	$\sim 30 \text{ min}$
Microfluidics <sup>38</sup> (Glass channel)	Photopolymerized monolith	hgDNA and whole blood	80 μL Max. 100 ng (DNA)	37–87%	1.8–86 ng	20 μL	$\sim 40 \text{ min}$
This study (PDMS channel)	Magnetic silica beads	Fish sperm DNA Hum. placenta DNA	10 μL Max. 370 μg (DNA)	~50%**	$\sim 80 \ \mu g/mg$ beads	60 μL (3 min)	~10 min**

<sup>\*</sup> This is the reported value by the manufacturer. An extraction efficiency of 62-68% <sup>53</sup> was reported for blood.

<sup>\*\*</sup> at optimum operating conditions (adsorption with 10  $\mu L/min$ , wash and desorption with 20  $\mu L/min$ )

#### References

- (1) Zhang, S.; Han, S.; Zhang, M.; Wang, Y. Non-invasive prenatal paternity testing using cell-free fetal DNA from maternal plasma: DNA isolation and genetic marker studies. Leg. Med. 2018, 32, 98–103.
- (2) Lewis, C. A.; Layne, T. R.; Seashols-Williams, S. J. Detection of microRNAs in DNA extractions for forensic biological source identification. <u>J. Forensic Sci.</u> 2019, <u>64</u>, 1823–1830.
- (3) Byrnes, S.; Bishop, J.; Lafleur, L.; Buser, J.; Lutz, B.; Yager, P. One-step purification and concentration of DNA in porous membranes for point-of-care applications. <u>Lab</u> Chip **2015**, 15, 2647–2659.
- (4) Roy, D.; Tiirikainen, M. Diagnostic power of DNA methylation classifiers for early detection of cancer. Trends Cancer **2020**, 6, 78–81.
- (5) Steppert, P.; Burgstaller, D.; Klausberger, M.; Berger, E.; Aguilar, P. P.; Schneider, T. A.; Kramberger, P.; Tover, A.; Nöbauer, K.; Razzazi-Fazeli, E. Purification of HIV-1 gag virus-like particles and separation of other extracellular particles. J. Chromatogr. A 2016, 1455, 93–101.
- (6) Moghanloo, G. M. M.; Khatami, M.; Javidanbardan, A.; Hosseini, S. N. Enhancing recovery of recombinant hepatitis B surface antigen in lab-scale and large-scale anion-exchange chromatography by optimizing the conductivity of buffers. <u>Protein Expr.</u> Purif. **2018**, 141, 25–31.
- (7) Balnis, J.; Madrid, A.; Hogan, K. J.; Drake, L. A.; Chieng, H. C.; Tiwari, A.; Vincent, C. E.; Chopra, A.; Vincent, P. A.; Robek, M. D. Blood DNA methylation and COVID-19 outcomes. Clin. Epigenetics **2021**, 13, 118.

- (8) McIntosh, N. L.; Berguig, G. Y.; Karim, O. A.; Cortesio, C. L.; De Angelis, R.; Khan, A. A.; Gold, D.; Maga, J. A.; Bhat, V. S. Comprehensive characterization and quantification of adeno associated vectors by size exclusion chromatography and multi angle light scattering. Sci. Rep. 2021, 11, 3012.
- (9) Olgun, H. B.; Tasyurek, H. M.; Sanlioglu, A. D.; Sanlioglu, S. High-grade purification of third-generation HIV-based lentiviral vectors by anion exchange chromatography for experimental gene and stem cell therapy applications. <u>Methods Mol Biol.</u> 2019, <u>1879</u>, 347–365.
- (10) Guo, J.; Lin, H.; Wang, J.; Lin, Y.; Zhang, T.; Jiang, Z. Recent advances in bio-affinity chromatography for screening bioactive compounds from natural products. <u>J. Pharm.</u> Biomed. Anal. **2019**, 165, 182–197.
- (11) Chong, K. W. Y.; Thong, Z.; Syn, C. K. Recent trends and developments in forensic DNA extraction. WIREs Forensic Sci. **2021**, 3, e1395.
- (12) Shi, R.; Panthee, D. R. A novel plant DNA extraction method using filter paper-based 96-well spin plate. Planta **2017**, 246, 579–584.
- (13) Hasap, L.; Chotigeat, W.; Pradutkanchana, J.; Asawutmangkul, W.; Kitpipit, T.; Thanakiatkrai, P. Comparison of two DNA extraction methods: PrepFiler® BTA and modified PCI-silica based for DNA analysis from bone. Forensic Sci. Int. Genet. Suppl. Ser. 2019, 7, 669–670.
- (14) He, Z.; Tang, C.; Chen, X.; Liu, H.; Yang, G.; Xiao, Z.; Li, W.; Deng, Y.; Jin, L.; Chen, H. Based on magnetic beads to develop the kit for extraction of high-quality cell-free DNA from blood of breast cancer patients. Mater. Express. **2019**, 9, 956–961.
- (15) Tan, S. C.; Yiap, B. C. DNA, RNA, and protein extraction: the past and the present. J. Biotechnol. Biomed. **2009**, 2009.

- (16) Dhaliwal, A. DNA extraction and purification. Mater. Methods 2013, 3, 191.
- (17) M Carpi, F.; Di Pietro, F.; Vincenzetti, S.; Mignini, F.; Napolioni, V. Human DNA extraction methods: patents and applications. <u>Recent Patents on DNA & Gene Sequences</u> **2011**, 5, 1–7.
- (18) Claassen, S.; du Toit, E.; Kaba, M.; Moodley, C.; Zar, H. J.; Nicol, M. P. A comparison of the efficiency of five different commercial DNA extraction kits for extraction of DNA from faecal samples. J. Microbiol. Methods **2013**, 94, 103–110.
- (19) Chacon-Cortes, D.; Haupt, L. M.; Lea, R. A.; Griffiths, L. R. Comparison of genomic DNA extraction techniques from whole blood samples: a time, cost and quality evaluation study. Mol. Biol. Rep. **2012**, 39, 5961–5966.
- (20) Queipo-Ortuno, M.; Tena, F.; Colmenero, J.; Morata, P. Comparison of seven commercial DNA extraction kits for the recovery of Brucella DNA from spiked human serum samples using real-time PCR. Eur. J. Clin. Microbiol. **2008**, 27, 109–114.
- (21) Tangchaikeeree, T.; Polpanich, D.; Elaissari, A.; Jangpatarapongsa, K. Magnetic particles for in vitro molecular diagnosis: From sample preparation to integration into microsystems. Colloids Surf. B **2017**, 158, 1–8.
- (22) Diefenbach, R. J.; Lee, J. H.; Kefford, R. F.; Rizos, H. Evaluation of commercial kits for purification of circulating free DNA. Cancer Genet. **2018**, 228, 21–27.
- (23) Tang, Y.; Zhang, J. Recent developments in DNA adduct analysis using liquid chromatography coupled with mass spectrometry. <u>J. Sep. Sci.</u> **2020**, <u>43</u>, 31–55.
- (24) Ayoib, A.; Hashim, U.; Gopinath, S. C.; Md Arshad, M. DNA extraction on bio-chip: history and preeminence over conventional and solid-phase extraction methods. <u>Appl.</u> Microbiol. Biotechnol. 101, 8077–8088.

- (25) Vicente, F. A.; Plazl, I.; Ventura, S. P.; Žnidaršič Plazl, P. Separation and purification of biomacromolecules based on microfluidics. Green Chem. **2020**, 22, 4391–4410.
- (26) Choe, S.-w.; Kim, B.; Kim, M. Progress of microfluidic continuous separation techniques for micro-/nanoscale bioparticles. Biosensors **2021**, 11, 464.
- (27) Ali, N.; Rampazzo, R. d. C. P.; Costa, A. D. T.; Krieger, M. A. Current nucleic acid extraction methods and their implications to point-of-care diagnostics. <u>Biomed. Res.</u> Int. **2017**, 2017.
- (28) Hatipoğlu, U.; Çetin, B.; Yıldırım, E. A novel zero-dead-volume sample loading interface for microfluidic devices: flexible hydraulic reservoir (FHR). <u>J. Micromech.</u> Microeng. **2018**, 28, 097001.
- (29) Atay, A.; Topuz, A.; Sarıarslan, B.; Yıldırım, E.; Charmet, J.; Couling, K.; Çetin, B. Flow rate-controlled pipetting for microfluidics: second-generation flexible hydraulic reservoir (FHRv2). Microfluid. Nanofluid. **2021**, 25, 3.
- (30) Pattanayak, P.; Singh, S. K.; Gulati, M.; Vishwas, S.; Kapoor, B.; Chellappan, D. K.; Anand, K.; Gupta, G.; Jha, N. K.; Gupta, P. K. Microfluidic chips: recent advances, critical strategies in design, applications and future perspectives. <u>Microfluid. Nanofluid.</u> **2021**, 25, 1–28.
- (31) Günal, G.; Kip, Ç.; Öğüt, S. E.; Usta, D. D.; Şenlik, E.; Kibar, G.; Tuncel, A. Human genomic DNA isolation from whole blood using a simple microfluidic system with silica-and polymer-based stationary phases. Mater. Sci. Eng. C **2017**, 74, 10–20.
- (32) Bao, B.; Wang, Z.; Thushara, D.; Liyanage, A.; Gunawardena, S.; Yang, Z.; Zhao, S. Recent advances in microfluidics-based chromatography—A mini review. <u>Separations</u> **2020**, 8, 3.

- (33) Geissler, M.; Brassard, D.; Clime, L.; Pilar, A. V. C.; Malic, L.; Daoud, J.; Barrère, V.; Luebbert, C.; Blais, B. W.; Corneau, N. Centrifugal microfluidic lab-on-a-chip system with automated sample lysis, DNA amplification and microarray hybridization for identification of enterohemorrhagic Escherichia coli culture isolates. <u>Analyst</u> 2020, <u>145</u>, 6831–6845.
- (34) Mauk, M. G.; Liu, C.; Sadik, M.; Bau, H. H. Microfluidic devices for nucleic acid (NA) isolation, isothermal NA amplification, and real-time detection. <u>Mobile Health</u> Technologies: Methods and Protocols **2015**, 15–40.
- (35) Dehghan, A.; Gholizadeh, A.; Navidbakhsh, M.; Sadeghi, H.; Pishbin, E. Integrated microfluidic system for efficient DNA extraction using on-disk magnetic stirrer micromixer. Sens. Actuators B Chem. **2022**, 351, 130919.
- (36) Cho, Y.-K.; Lee, J.-G.; Park, J.-M.; Lee, B.-S.; Lee, Y.; Ko, C. One-step pathogen specific DNA extraction from whole blood on a centrifugal microfluidic device. <u>Lab</u> Chip **2007**, 7, 565–573.
- (37) Jackson, K. R.; Borba, J. C.; Meija, M.; Mills, D. L.; Haverstick, D. M.; Olson, K. E.; Aranda, R.; Garner, G. T.; Carrilho, E.; Landers, J. P. DNA purification using dynamic solid-phase extraction on a rotationally-driven polyethylene-terephthalate microdevice.

  <u>Analytica Chimica Acta</u> **2016**, 937, 1–10.
- (38) Wen, J.; Guillo, C.; Ferrance, J. P.; Landers, J. P. Microfluidic-Based DNA Purification in a Two-Stage, Dual-Phase Microchip Containing a Reversed-Phase and a Photopolymerized Monolith. Anal. Chem. **2007**, 79, 6135–6142.
- (39) Ayoib, A.; Hashim, U.; Gopinath, S. C. Automated, high-throughput DNA extraction protocol for disposable label free, microfluidics integrating DNA biosensor for oil palm pathogen, Ganoderma boninense. Process Biochem. **2020**, 92, 447–456.

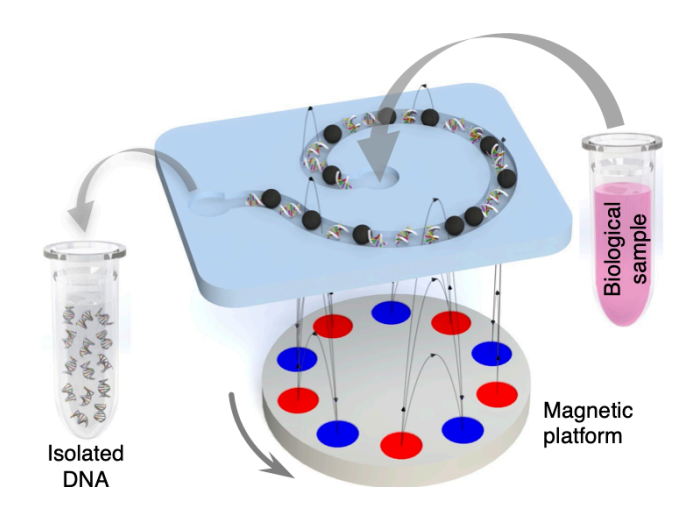
- (40) Liu, J.; Zhao, J.; Petrochenko, P.; Zheng, J.; Hewlett, I. Sensitive detection of influenza viruses with Europium nanoparticles on an epoxy silica sol-gel functionalized polycarbonate-polydimethylsiloxane hybrid microchip. <u>Biosens. Bioelectron.</u> **2016**, <u>86</u>, 150–155.
- (41) Zhou, W.; Dou, M.; Timilsina, S. S.; Xu, F.; Li, X. Recent innovations in cost-effective polymer and paper hybrid microfluidic devices. Lab Chip **2021**, 21, 2658–2683.
- (42) Zhang, X.; Wu, X.; Peng, R.; Li, D. Electromagnetically controlled microfluidic chip for DNA extraction. Measurement **2015**, 75, 23–28.
- (43) Gauri, S.; Gan, K. B.; Then, S.-M. Simulation of DNA extraction and separation from salivary fluid by superparamagnetic beads and electromagnetic field in microfluidic platform. Microsyst. Technol. **2019**, 25, 1379–1385.
- (44) Zhu, Y.; Zhang, B.; Gu, J.; Li, S. Magnetic beads separation characteristics of a microfluidic bioseparation chip based on magnetophoresis with lattice-distributed soft magnets. J. Magn. Magn. Mater. **2020**, 501, 166485.
- (45) Serra, M.; Mai, T. D.; Serra, A.; Nguyen, M.-C.; Eisele, A.; Perié, L.; Viovy, J.-L.; Ferraro, D.; Descroix, S. Integrated droplet microfluidic device for magnetic particles handling: Application to DNA size selection in NGS libraries preparation. <u>Sens.</u> Actuators B Chem. **2020**, 305, 127346.
- (46) Hale, C.; Darabi, J. Magnetophoretic-based microfluidic device for DNA isolation. Biomicrofluidics **2014**, 8, 044118.
- (47) Doganay, S.; Cetin, L.; Ezan, M. A.; Turgut, A. A rotating permanent magnetic actuator for micropumping devices with magnetic nanofluids. <u>J. Micromech. Microeng.</u> **2020**, 30, 075012.
- (48) Coey, J. Permanent magnet applications. J. Magn. Magn. Mater. 2002, 248, 441–456.

- (49) Xu, Y.; Zhang, Z.; Su, Z.; Zhou, X.; Han, X.; Liu, Q. Continuous microfluidic purification of DNA using magnetophoresis. Micromachines **2020**, 11, 187.
- (50) Lee, H.; Kim, G.; Park, E.; Jeon, S. Lenz's law-based virtual net for detection of pathogenic bacteria from water. Anal. Chem. **2019**, 91, 15585–15590.
- (51) Saadat, M.; Shafii, M. B.; Ghassemi, M. Numerical investigation on mixing intensification of ferrofluid and deionized water inside a microchannel using magnetic actuation generated by embedded microcoils for lab-on-chip systems. <u>Chem. Eng. Process</u> Process Intensif. 2020, 147, 107727.
- (52) Lund-Olesen, T.; Dufva, M.; Hansen, M. F. Capture of DNA in microfluidic channel using magnetic beads: Increasing capture efficiency with integrated microfluidic mixer. J. Magn. Magn. Mater. 2007, 311, 396–400.
- (53) Duarte, G. R. M.; Price, C. W.; Littlewood, J. L.; Haverstick, D. M.; Ferrance, J. P.; Carrilho, E.; Landers, J. P. Characterization of dynamic solid phase DNA extraction from blood with magnetically controlled silica beads. Analyst **2010**, 135, 531–537.
- (54) Azimi, S. M.; Nixon, G.; Ahern, J.; Balachandran, W. A magnetic bead-based DNA extraction and purification microfluidic device. <u>Microfluid. Nanofluid.</u> 2011, <u>11</u>, 157–165.
- (55) Xiong, Q.; Lim, C. Y.; Ren, J.; Zhou, J.; Pu, K.; Chan-Park, M. B.; Mao, H.; Lam, Y. C.; Duan, H. Magnetic nanochain integrated microfluidic biochips. <u>Nat. Commun.</u> 2018, 9, 1743.
- (56) Karle, M.; Miwa, J.; Czilwik, G.; Auwärter, V.; Roth, G.; Zengerle, R.; von Stetten, F. Continuous microfluidic DNA extraction using phase-transfer magnetophoresis. <u>Lab</u> Chip **2010**, 10, 3284–3290.

- (57) Hung, P.-Y.; Jiang, P.-S.; Lee, E.-F.; Fan, S.-K.; Lu, Y.-W. Genomic DNA extraction from whole blood using a digital microfluidic (DMF) platform with magnetic beads. Microsyst. Technol. **2017**, 23, 313–320.
- (58) Hatipoğlu, U.; Kibar, G.; Çetin, B. Enrichment of samples inside microchannels by using magnetic particles. Int. Patent Appl. No: PCT/TR2019/050728, 2019; https://patents.google.com/patent/W02020050809A2/en.
- (59) Günal, G.; Kip, Ç.; Eda Öğüt, S.; İlhan, H.; Kibar, G.; Tuncel, A. Comparative DNA isolation behaviours of silica and polymer based sorbents in batch fashion: monodisperse silica microspheres with bimodal pore size distribution as a new sorbent for DNA isolation. Artif. Cells Nanomed. Biotechnol. **2018**, 46, 178–184.
- (60) Salimi, K.; Usta, D. D.; Çelikbiçak, Ö.; Pinar, A.; Salih, B.; Tuncel, A. Ti(IV) carrying polydopamine-coated, monodisperse-porous SiO2 microspheres with stable magnetic properties for highly selective enrichment of phosphopeptides. <u>Colloids Surf. B</u> 2017, 153, 280–290.
- (61) Kibar, G.; Topal, A. E.; Dana, A.; Tuncel, A. Newly designed silver coated-magnetic, monodisperse polymeric microbeads as SERS substrate for low-level detection of amoxicillin. J. Mol. Struct. 2016, 1119, 133–138.
- (62) Rasooli, R.; Çetin, B. Assessment of Lagrangian modeling of particle motion in a spiral microchannel for inertial microfluidics. Micromachines **2018**, 9, 433.
- (63) Düven, G.; Çetin, B.; Kurtuldu, H.; Gündüz, G. T.; Tavman, Ş.; Kışla, D. A portable microfluidic platform for rapid determination of microbial load and somatic cell count in milk. Biomed. Microdev. **2019**, 21, 49.
- (64) Kibar, G.; Çalışkan, U.; Erdem, E. Y.; Çetin, B. One-pot synthesis of organic-inorganic hybrid polyhedral oligomeric silsesquioxane microparticles in a double-zone temperature

- controlled microfluidic reactor. <u>J. Polym. Sci., Part A: Polym. Chem.</u> **2019**, <u>57</u>, 1396–1403.
- (65) Thermo Fisher Scientific Inc., NanoDrop 2000/2000c Spectrophotometer V1.0 User Manual. https://assets.thermofisher.com/TFS-Assets/CAD/manuals/NanoDrop-2000-User-Manual-EN.pdf, 2009; Accessed: December 29, 2023.
- (66) Wang, J.; Guo, X. Adsorption isotherm models: Classification, physical meaning, application and solving method. Chemosphere **2020**, 258, 127279.
- (67) Kibar, G. Effect of Crosslinking Agent on Mesoporous Spherical POSS Hybrid Particles: Synthesis, Characterization and Thermal Stability. <u>J. Inorg. Organomet. Polym. Mater.</u> 2023, 33, 831–840.
- (68) Li, X.; Zhang, J.; Gu, H. Adsorption and desorption behaviors of DNA with magnetic mesoporous silica nanoparticles. Langmuir **2011**, 27, 6099–6106.
- (69) Gómez Pérez, A.; González-Martínez, E.; Díaz Águila, C. R.; González-Martínez, D. A.; González Ruiz, G.; García Artalejo, A.; Yee-Madeira, H. Chitosan-coated magnetic iron oxide nanoparticles for DNA and rhEGF separation. Colloids Surf. A **2020**, 591, 124500.
- (70) Niu, B.; Zhou, Y.; Wen, T.; Quan, G.; Singh, V.; Pan, X.; Wu, C. Proper functional modification and optimized adsorption conditions improved the DNA loading capacity of mesoporous silica nanoparticles. <u>Colloids Surf. A: Physicochem. Eng.</u> 2018, <u>548</u>, 98–107.
- (71) Pan, X.; Cheng, S.; Su, T.; Zuo, G.; Zhang, C.; Wu, L.; Jiao, Y.; Dong, W. Poly (2-hydroxypropylene imines) functionalized magnetic polydopamine nanoparticles for high-efficiency DNA isolation. Appl. Surf. Sci. **2019**, 498, 143888.
- (72) Ghaemi, M.; Absalan, G. Study on the adsorption of DNA on Fe3O4 nanoparticles and on ionic liquid-modified Fe3O4 nanoparticles. Microchim. Acta **2014**, 181, 45–53.

- (73) Tanaka, T.; Sakai, R.; Kobayashi, R.; Hatakeyama, K.; Matsunaga, T. Contributions of Phosphate to DNA Adsorption/Desorption Behaviors on Aminosilane-Modified Magnetic Nanoparticles. Langmuir 2009, 25, 2956–2961.
- (74) Shan, Z.; Jiang, Y.; Guo, M.; Bennett, J. C.; Li, X.; Tian, H.; Oakes, K.; Zhang, X.; Zhou, Y.; Huang, Q.; Chen, H. Promoting DNA loading on magnetic nanoparticles using a DNA condensation strategy. Colloids Surf. B **2015**, 125, 247–254.
- (75) Wen, J.; Legendre, L. A.; Bienvenue, J. M.; Landers, J. P. Purification of Nucleic Acids in Microfluidic Devices. Anal. Chem. **2008**, 80, 6472–6479.



For Table of Contents Only